EPJ Web of Conferences **130**, 01028 (2016) DOI: 10.1051/epjconf/201613001028
MESON 2016

Quarkonium and heavy flavour meson production at 13 TeV at ATLAS

Leonid Gladilin[1,⋆]
for the ATLAS Collaboration

[1] *Lomonosov Moscow State University Skobeltsyn Institute of Nuclear Physics (SINP MSU), Moscow 119991, Russian Federation*

Abstract. First results of the ATLAS experiment at LHC on quarkonium and heavy flavour meson production in proton-proton collisions at 13 TeV are presented. A brief summary of the results obtained at 7-8 TeV is also reported. Comparison of the data cross sections with various theoretical predictions is discussed.

1 Introduction

Measurements of the charmed and beauty mesons production and the non-prompt (from b-hadron decays) production of charmonium states probe production and hadronisation of c and b quarks. Measurements of the bottomonium and prompt charmonium production probe a heavy quark pair production and its subsequent evolution into a bound state. The latter includes non-perturbative effects and can be described with colour-singlet (CS) and colour-octet (CO) contributions in the framework of non-relativistic QCD (NRQCD). In this framework, the non-perturbative evolution is described with long-distance matrix elements (LDME) tuned to experimental results. First results on quarkonium and heavy flavour meson production in proton-proton collisions at 13 TeV and recent results at 7-8 TeV obtained with the ATLAS [1] detector at the LHC are described in this note.

2 Charmonium production

The non-prompt J/ψ production fraction has been measured differentially as a function of the J/ψ transverse momentum and rapidity using 6.4 pb^{-1} of proton-proton collision data at a centre-of-mass energy of 13 TeV [2]. The fraction in intervals of dimuon p_{T} and $|y|$ is measured and summarised in Fig. 1(left). The non-prompt fraction is found to increase steadily from 0.25 at a transverse momentum of 8 GeV to 0.65 at 40 GeV, with no significant variation with rapidity observed within the precision of the measurement. The centre-of-mass energy (and initial-state) dependence of the fraction is studied by comparing these results, in the J/ψ rapidity interval $|y| < 0.75$, to previous ATLAS measurements in the same rapidity region at $\sqrt{s} = 2.76$ TeV and a comparable rapidity interval ($0.25 < |y| < 0.50$) at $\sqrt{s} = 7$ TeV, and CDF measurements in a slightly different rapidity interval ($|y| < 0.6$) at $\sqrt{s} = 1.96$ TeV. The comparison is illustrated in Fig. 1(right). No significant change in the non-prompt

⋆e-mail: gladilin@mail.cern.ch

fraction is observed from $\sqrt{s} = 7$ TeV to $\sqrt{s} = 13$ TeV, contrary to the significant difference observed between the $\sqrt{s} = 7$ TeV measurement and the measurements at lower energies.

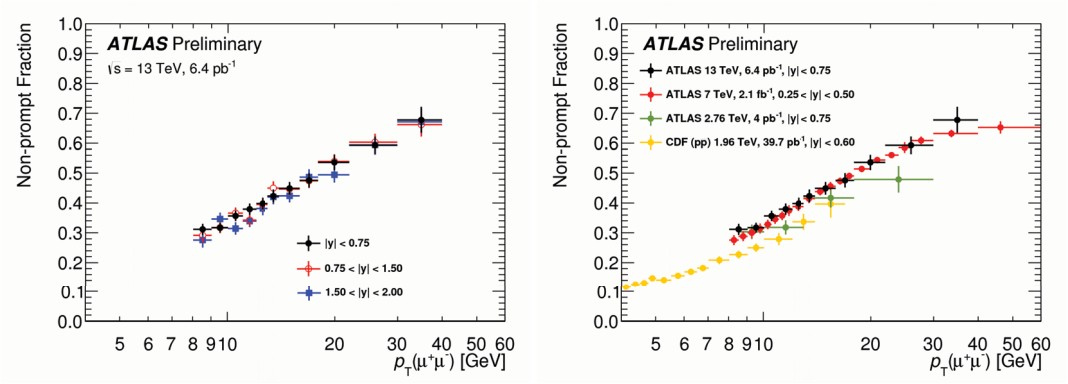

Figure 1. Non-prompt J/ψ production fraction as a function of J/ψ p_{T} in (left) three intervals of J/ψ rapidity and in (right) the most central rapidity region ($|y| < 0.75$) [2] compared to previous measurements from ATLAS in pp collisions at 2.76 GeV and 7 GeV, and from CDF in $p\bar{p}$ collisions at $\sqrt{s} = 1.96$ GeV.

Differential cross sections of the charmonium prompt and non-prompt production have been measured in pp collisions at $\sqrt{s}$ = 7-8 TeV for the $J/\psi \to \mu^+\mu^-$ and $\psi(2S) \to \mu^+\mu^-$ [3], $\psi(2S) \to J/\psi\pi^+\pi^-$ [4, 5], $\chi_{c1/2} \to J/\psi\gamma$ [6] and $X(3872) \to J/\psi\pi^+\pi^-$ [5] final states.

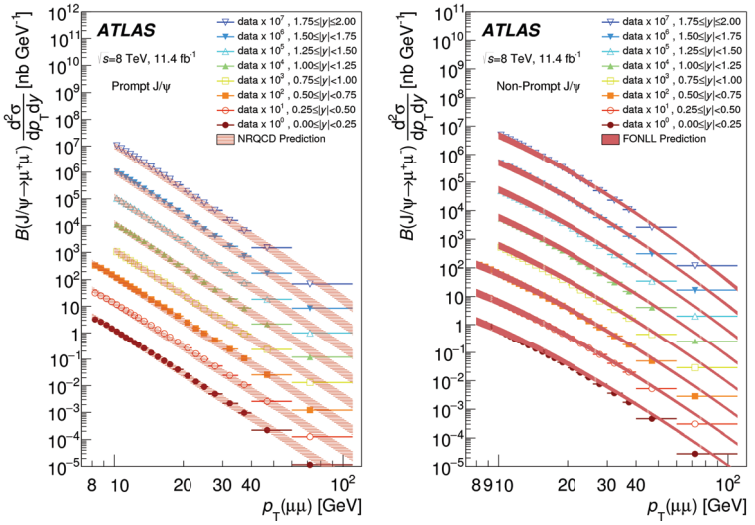

Figure 2. The differential (left) prompt and (right) non-prompt cross section times dimuon branching fraction of J/ψ as a function of J/ψ p_{T} for eight slices in rapidity [3]. For each increasing rapidity slice, an additional scaling factor of 10 is applied to the plotted points for visual clarity. Theoretical predictions are also shown.

Figure 2 shows the differential prompt and non-prompt cross section times dimuon branching fraction of J/ψ as a function of J/ψ p_{T} for eight slices in rapidity. For the prompt production, predictions from the NRQCD model, which includes colour-octet contributions with LDMEs tuned to earlier collider data, are in good agreement with the data. For the non-prompt production, the fixed-order next-to-leading-logarithm (FONLL) calculations reproduce the data reasonably well, with a

slight overestimation of the differential cross sections at the highest transverse momenta. Similar conclusions have been done for prompt and non-prompt production of $\psi(2S)$ and $\chi_{c1/2}$.

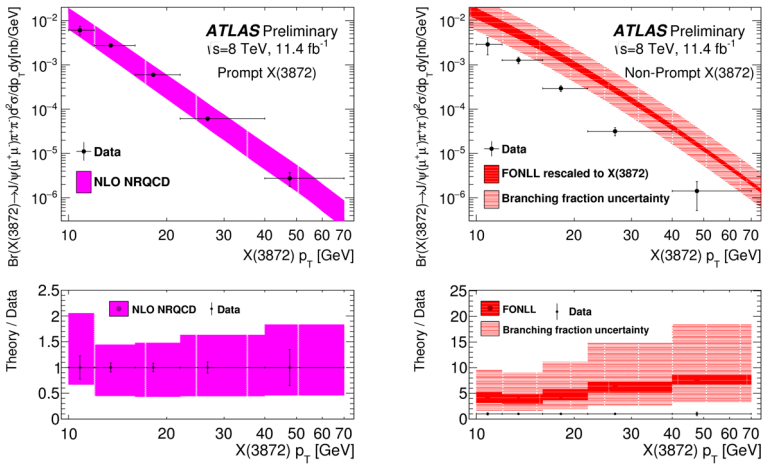

Figure 3. The differential (left) prompt and (right) non-prompt cross section times branching fractions of $X(3872)$ as a function of $X(3872)$ p_{T} [5]. Theoretical predictions are also shown.

Figure 3 shows differential prompt and non-prompt cross section times branching fractions of $X(3872)$ as a function of $X(3872)$ p_{T}. For the prompt production, good agreement is found with theoretical predictions within the NLO NRQCD model, which considers $X(3872)$ to be a mixture of $\chi_{c1}(2P)$ and a $D^0\bar{D}^{*0}$ molecular state, with the production being dominated by the $\chi_{c1}(2P)$ component and the normalisation fixed through the fit to the earlier LHC data. For the non-prompt production, the FONLL calculations for $\psi(2S)$, recalculated for X(3872) using the branching fraction $Br(B \to X(3872))Br(X(3872) \to J/\psi\pi^+\pi^-) = (1.9 \pm 0.8) \times 10^{-4}$ estimated in [7] from the Tevatron data, overestimate the data, especially at large transverse momenta.

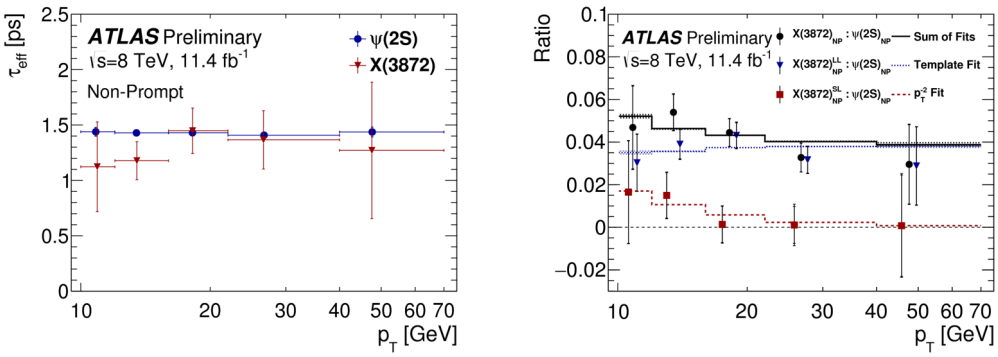

Figure 4. Measured (left) effective pseudo-proper lifetimes for non-prompt $\psi(2S)$ and $X(3872)$ and (right) ratio of cross section times branching fraction between $X(3872)$ and $\psi(2S)$ for non-prompt production [5]. In (right), the total non-prompt ratio (black circles) is separated into short-lived (red squares) and long-lived (blue triangles) components for the $X(3872)$, shown with respective fits described in the text.

Figure 4(left) shows measured effective pseudo-proper lifetimes for non-prompt $\psi(2S)$ and $X(3872)$. While the pseudo-proper lifetime distribution is nearly flat for $\psi(2S)$, the signal from $X(3872)$ at low p_{T} tends to have shorter lifetimes. The non-prompt production cross section of $X(3872)$ is split into long-lived ($\tau = 1.45 \pm 0.05$ ps) and short-lived ($\tau = 0.40 \pm 0.05$ ps) components. Figure 4(right) shows ratio of cross section times branching fraction between $X(3872)$ and $\psi(2S)$ for the total non-prompt production and for the long-lived and short-lived components. The measured ratio of long-lived $X(3872)$ is well described by the Monte Carlo kinematic template which is nearly flat. The short-lived component can originate from B_c production, which is expected to be dominated by non-fragmentation processes at low transverse momentum [8]. These processes are expected to have p_{T} dependence $\propto p_{\mathrm{T}}^{-2}$ relative to the fragmentation contribution. So the ratio of short-lived non-prompt $X(3872)$ to non-prompt $\psi(2S)$ is fitted with a function a/p_{T}^2 to find $a = 2.04 \pm 1.43(stat) \pm 0.34(sys)\,\mathrm{GeV}^2$ [5]. This value is used to determine the fraction of the short-lived component in the non-prompt $X(3872)$ production, for $p_{\mathrm{T}} > 10\,\mathrm{GeV}$, to be $(25 \pm 13(stat) \pm 2(sys) \pm 5(spin))\%$ [5], where the last uncertainty comes from the variation of the spin alignment of $X(3872)$.

3 Beauty and charmed meson production

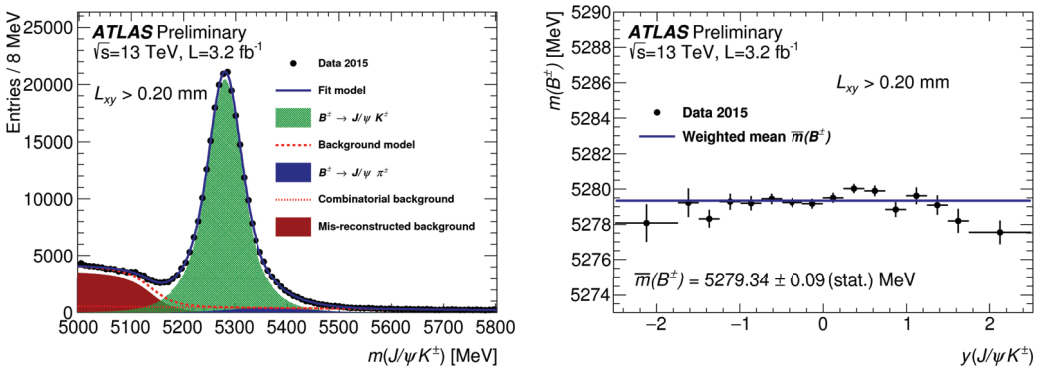

Figure 5. B^+ mass (left) reconstructed for all $B^+ \to J/\psi K^+$ candidates and (right) fitted in several bins of $y(B^+)$ [9].

The performance of B^+ mass reconstruction in $B^+ \to J/\psi K^+$ decay at 13 TeV is verified using $3.2\,\mathrm{fb}^{-1}$ of pp collision data [9]. Figure 5 shows the B^+ mass reconstructed for all $B^+ \to J/\psi K^+$ candidates and fitted in several bins of $y(B^+)$. The measured B^+ mass is in good agreement with the world average value.

The strangeness-suppression factor, $\gamma_{s/d}$, in beauty fragmentation is determined, using decays $B_s^0 \to J/\psi\phi$ and $B_d^0 \to J/\psi K^{0*}$, to be $(0.240 \pm 0.004(stat) \pm 0.010(sys) \pm 0.017(th))\%$ [10], where the last uncertainty is due to the uncertainty of the perturbative QCD prediction for $Br(B_s^0 \to J/\psi\phi)/Br(B_d^0 \to J/\psi K^{0*})$ [11].

The differential cross section for B^+ meson production has been studied with $2.4\,\mathrm{fb}^{-1}$ of pp collision data at 7 TeV [12]. The FONLL calculations reproduce the data reasonably well.

The production of $D^{*\pm}$, $D^{\pm}$ and $D_s^{\pm}$ charmed mesons has been measured in the kinematic region $3.5 < p_{\mathrm{T}}(D) < 100\,\mathrm{GeV}$ and $|\eta(D)| < 2.1$ in pp collisions at 7 TeV, using an integrated luminosity of

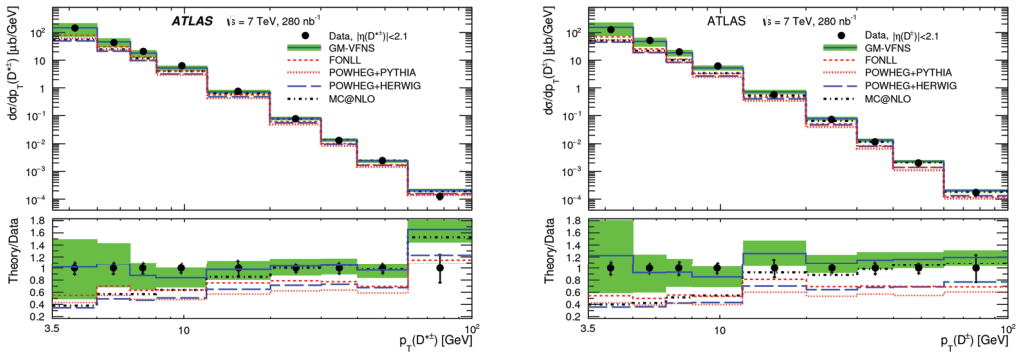

Figure 6. Differential cross sections for (left) $D^{*\pm}$ and (right) $D^{\pm}$ mesons as a function of p_{T} for data (points) [13] compared to the NLO QCD calculations of FONLL, POWHEG+PYTHIA, POWHEG+HERWIG, MC@NLO and GM-VFNS (histograms). The bands show the estimated theoretical uncertainty of the GM-VFNS calculation.

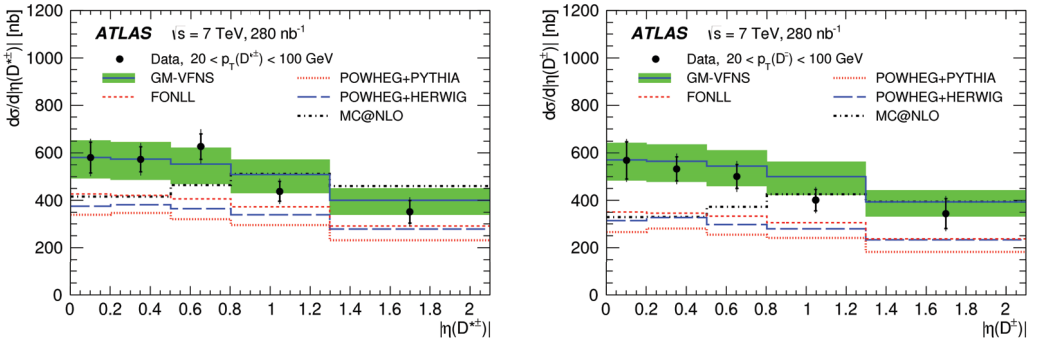

Figure 7. Differential cross sections for (left) $D^{*\pm}$ and (right) $D^{\pm}$ mesons as a function of $|\eta|$ for data (points) [13] compared to the NLO QCD calculations of FONLL, POWHEG+PYTHIA, POWHEG+HERWIG, MC@NLO and GM-VFNS (histograms). The bands show the estimated theoretical uncertainty of the GM-VFNS calculation.

up to 280 nb^{-1} [13]. Figures 6-7 show differential cross sections for $D^{*\pm}$ and $D^{\pm}$ mesons as functions of p_{T} and $|\eta(D)|$ for data compared to the NLO QCD calculations. The FONLL, POWHEG+PYTHIA and POWHEG+HERWIG predictions are generally below the data. They are consistent with the data in the measured $p_{\mathrm{T}}(D)$ and $|\eta(D)|$ ranges within the large theoretical uncertainties. The FONLL and POWHEG predictions reproduce the shapes of the data distributions. The p_{T} shape of the MC@NLO prediction is harder than that for the data. The $|\eta|$ shape of the MC@NLO prediction in the range $20 < p_{\mathrm{T}} < 100$ GeV differs from the data and all other predictions. The general-mass variable-flavour-number scheme (GM-VFNS) predictions agree with data in both shape and normalisation.

The visible D cross sections are extrapolated to the cross sections in the full kinematic phase space after subtracting the cross-section fractions originating from beauty production. To calculate the total cross section of charm production, the total production cross section of a given D meson should be divided by twice the value of the corresponding charm fragmentation fraction [14]. The weighted

mean of the two values calculated from $D^{*\pm}$ and $D^{\pm}$ cross sections is [13]:

$$\sigma^{\mathrm{tot}}_{c\bar{c}} = 8.6 \pm 0.3(stat) \pm 0.7(sys) \pm 0.3(lum) \pm 0.2(ff)^{+3.8}_{-3.4}(extr)\,\mathrm{mb},$$

where the fourth uncertainty is due to the uncertainty of the fragmentation fractions and the last uncertainty is due to the extrapolation procedure. The total cross section of charm production agree with the result of the ALICE collaboration.

The total cross sections for D production are also used to calculate two fragmentation ratios for charged charmed mesons: the strangeness-suppression factor, $\gamma_{s/d}$, and the fraction of charged non-strange D mesons produced in a vector state, P^d_{v} [13]:

$$\gamma_{s/d} = 0.26 \pm 0.05(stat) \pm 0.02(sys) \pm 0.02(br) \pm 0.01(extr),$$

$$P^d_{\mathrm{v}} = 0.56 \pm 0.03(stat) \pm 0.01(sys) \pm 0.01(br) \pm 0.02(extr).$$

The fragmentation ratios agree with those obtained by the ALICE collaboration at the LHC, and those measured in e^+e^- annihilations at LEP and in $e^{\pm}p$ collisions at HERA. The value of strangeness-suppression in charm fragmentation agrees with that measured in beauty fragmentation.

Acknowledgments

Participation in the conference was supported by the Russian Foundation for Basic Research, grant 15-02-08133.

References

[1] ATLAS Collaboration, JINST **3**, S08003 (2008)
[2] ATLAS Collaboration, ATLAS-CONF-2015-030, http://cds.cern.ch/record/2037967 (2015)
[3] ATLAS Collaboration, Eur. Phys. J. **76**, 283 (2016)
[4] ATLAS Collaboration, JHEP **09**, 079 (2014)
[5] ATLAS Collaboration, ATLAS-CONF-2016-028, http://cds.cern.ch/record/2160169 (2016)
[6] ATLAS Collaboration, JHEP **07**, 154 (2014)
[7] P. Artoisenet and E. Braaten, Phys. Rev. D **81**, 114018 (2010)
[8] A. V. Berezhnoy and A. K. Likhoded, arXiv:1309.1979 (2013)
[9] ATLAS Collaboration, ATLAS-CONF-2015-064, http://cds.cern.ch/record/2114830 (2015)
[10] ATLAS Collaboration, Phys. Rev. Lett. **115**, 262001 (2015)
[11] X. Liu, W. Wang and Y. Xie, Phys. Rev. D **89**, 094010 (2014)
[12] ATLAS Collaboration, JHEP **10**, 042 (2013)
[13] ATLAS Collaboration, Nucl. Phys. B **907**, 717 (2016)
[14] L. Gladilin, Eur. Phys. J. C **75**, 19 (2015)